

# UC San Diego

## UC San Diego Previously Published Works

### Title

Manipulation of competing ferromagnetic and antiferromagnetic domains in exchange-biased nanostructures

### Permalink

<https://escholarship.org/uc/item/7985n837>

### Journal

Physical Review B, 92(17)

### ISSN

2469-9950

### Authors

Rodríguez, Arantxa Fraile  
Basaran, Ali C  
Morales, Rafael  
[et al.](#)

### Publication Date

2015-11-01

### DOI

10.1103/physrevb.92.174417

Peer reviewed

# Manipulation of competing ferromagnetic and antiferromagnetic domains in exchange-biased nanostructures

Arantxa Fraile Rodríguez,<sup>1,\*</sup> Ali C. Basaran,<sup>2</sup> Rafael Morales,<sup>3,4</sup> Miroslavna Kovylna,<sup>1</sup> Jordi Llobet,<sup>5</sup> Xavier Borrise,<sup>6</sup>

Matthew A. Marcus,<sup>7</sup> Andreas Scholl,<sup>7</sup> Ivan K. Schuller,<sup>2</sup> Xavier Batlle,<sup>1</sup> and Amílcar Labarta<sup>1</sup>

<sup>1</sup>*Departament de Física Fonamental and Institut de Nanociència i Nanotecnologia (IN2UB), Universitat de Barcelona, 08028 Barcelona, Spain*

<sup>2</sup>*Department of Physics and Center for Advanced Nanoscience, University of California San Diego, La Jolla, California 92093, USA* <sup>3</sup>*Department of Chemical-Physics, BC Materials, University of the Basque Country UPV/EHU, 48940 Leioa, Spain*

<sup>4</sup>*IKERBASQUE, Basque Foundation for Science, 48011 Bilbao, Spain*

<sup>5</sup>*Institut de Microelectrònica de Barcelona (IMB-CNM CSIC), 08193 Bellaterra, Spain*

<sup>6</sup>*Institut Català de Nanociència i Nanotecnologia (ICN2), Campus UAB, 08193 Bellaterra, Spain*

<sup>7</sup>*Advanced Light Source, Lawrence Berkeley National Laboratory, Berkeley, California 94720, USA*

(Received 4 March 2015; revised manuscript received 3 October 2015; published 20 November 2015)

with complex noncollinear FM/AF spin structures.

PACS number(s): 75.70.Cn, 75.60.Ch, 68.37.Yz

## I. INTRODUCTION

Geometric confinement of magnetic structures at length scales such as the ferromagnetic (FM) exchange length or domain wall width produces intriguing new phenomena not observed in the corresponding bulk material. In particular, exchange bias (EB), i.e., the unidirectional anisotropy induced in FM films by the proximity with an antiferromagnetic (AF) layer upon cooling through the AF Neel temperature ( $T_N$ ), is of particular interest [1–3]. The EB effect has become crucial for numerous applications such as spin valves [3], information storage [3,4], and electrically writable spintronics devices [5]. Recently, FM/AF nanostructures exhibiting simultaneous negative [1] and positive [6–10] EB (NEB, PEB, respectively), i.e., double hysteresis loops with the two subloops shifted against and along the cooling field direction, have been proposed for multistate switching memory [11,12]. This sign of EB can be controlled by either the cooling field or by changes in the domain configuration in both the AF bulk and at the FM/AF interface [7,8,13–15]. Moreover, patterning provides control over the writing fields and the design of the multistate cells [12]. For all of the above applications, robust, tunable EB heterostructures are required.

From a fundamental point of view, a detailed and quantitative description of the micromagnetic structure of FM/AF interfaces is essential to understand the EB phenomenon. Most theoretical models assume a well-established, temperature-

dependent AF spin configuration that is different between polycrystalline or epitaxial materials, compensated or uncompensated interfaces, and low or high AF anisotropy [16–21]. Furthermore, the AF domain structure has been so far mostly assumed to be insensitive to the neighboring FM, i.e., explained exclusively in terms of AF length scales and thus determined by inherent AF defect distributions, grain boundaries, step edges, or pinning centers [1–3]. In most of the experiments, the AF structure is usually set by field cooling (FC) across  $T_N$  [10,22–25] and the influence of the magnetic state of the adjacent FM layer is often disregarded.

We choose  $\text{FeF}_2$  as the AF because it has a simple crystal structure (body-centered tetragonal) [26], a collinear spin structure with the  $\text{Fe}^{2+}$  ions at the center of the unit cell ordering AF with respect to those at the corners [27,28], and a very strong uniaxial magnetic anisotropy ( $K \sim 1.39 \times 10^8$  erg/cm<sup>3</sup>) along the [001] c axis [29]. Because of its large anisotropy,  $\text{FeF}_2$  behaves as an Ising model system over a wide temperature range [30]. When grown epitaxially onto  $\text{MgF}_2$  (110) single-crystal substrates, the easy axis of  $\text{FeF}_2$  is collinearly aligned to the moments of the above FM since the [001] direction coincides with the growth-induced easy axis of the FM layer [7]. Ni/ $\text{FeF}_2$  bilayers provide a model EB system showing coexistence of negative and positive EB domains, i.e., AF regions for which the pinned uncompensated AF spins induce positive and negative unidirectional anisotropy in the FM. A number of studies have reported on the relationship between EB and AF domain size [25], the uncompensated moments in the AF and their coupling to the adjacent FM [22–24,31], the effect of patterning on the coexistence of

\*Corresponding author: arantxa.fraile@ub.edu

1098-0121/2015/92(17)/174417(7)

©2015 American Physical Society

Using photoemission electron microscopy combined with x-ray magnetic circular dichroism we show that a progressive spatial confinement of a ferromagnet (FM), either through thickness variation or laterally via patterning, actively controls the domains of uncompensated spins in the antiferromagnet (AF) in exchange-biased systems. Direct observations of the spin structure in both sides of the FM/AF interface in a model system, Ni/ $\text{FeF}_2$ , show that the spin structure is determined by the balance between the competing FM and AF magnetic energies. Coexistence of exchange bias domains, with opposite directions, can be established in Ni/ $\text{FeF}_2$  bilayers for Ni thicknesses below 10 nm. Patterning the Ni/ $\text{FeF}_2$  heterostructures with antidots destabilizes the FM state, enhancing the formation of opposite exchange bias domains below a critical antidot separation of the order of a few  $\text{FeF}_2$  crystal domains. The results suggest that dimensional confinement of the FM may be used to manipulate the AF spin structure in spintronic devices and ultrahigh-density information storage media. The underlying mechanism of the uncompensated AF domain formation in Ni/ $\text{FeF}_2$  may be generic to other magnetic systems

NEB and PEB [14,15], and the influence of the FM on the domain structure of the adjacent AF [31,32]. However, a deep understanding of how a systematic variation in the spatial confinement of the FM controls the AF spin structure is still missing.

In this work, we demonstrate that the spatial confinement of the FM can drastically affect the domains of uncompensated spins in the AF, even when the FM is fully saturated above the AF Neel temperature ( $T_N$ ). Direct observations of the spin configuration in both sides of the FM/AF interface using photoemission electron microscopy (PEEM) combined with x-ray magnetic circular dichroism (XMCD) prove that the final spin structure is determined by

the balance between the competing FM and AF magnetic energies. A coexistence of EB domains with opposite orientations can be monotonically tuned in Ni/ $\text{FeF}_2$  bilayers below 10 nm Ni thicknesses. Patterning these with antidots which laterally confine the EB domains yields an increase of opposite EB domains below a critical antidot separation of about 400 nm (of the order of a few  $\text{FeF}_2$  crystal domains [25,33]). These results imply that dimensional constrictions in the FM layer may be used to tune the AF spin structure in spintronic devices and ultrahigh-density information storage media.

## II. EXPERIMENTAL METHODS

The Ni/FeF<sub>2</sub> heterostructures were deposited by electron beam evaporation onto MgF<sub>2</sub> (110) single-crystal substrates, with a 2 nm Al capping layer to prevent oxidation, using a base pressure of  $3 \times 10^{-7}$  mbar, a deposition rate of  $1 \text{ \AA s}^{-1}$ , and deposition temperatures of 300°C for FeF<sub>2</sub> and 150°C for Ni and Al. The continuous bilayers consisted of 70-nm-thick FeF<sub>2</sub> and Ni thicknesses in the range of 0–11 nm. From x-ray diffraction and transmission electron microscopy (TEM) measurements, one can identify that the FeF<sub>2</sub> films grow epitaxial and untwinned along the (110) plane, whereas Ni is polycrystalline. FeF<sub>2</sub> (110) has a single AF easy axis lying in-plane along the [001] direction [7,34], with crystal domains of about 30 nm [25,33]. The growth-induced easy magnetization axis of the Ni layer coincides with the AF easy axis of FeF<sub>2</sub> [7]. High-resolution TEM images reveal smooth, highly crystalline FM/AF interfaces with few stacking faults and dislocations over the whole sample (see Figs. S1 and S2, Supplemental Material [35]). Square arrays of square antidots were patterned by focused ion beam lithography using an ion beam current of 30 pA through the whole depth of the Al(2nm)/Ni(6nm)/FeF<sub>2</sub>(70nm) heterostructures [14,36]. The antidots, with in-plane edges parallel and perpendicular to the [001] FeF<sub>2</sub> crystal direction, have close to 200 nm edge length and edge-to-edge separation around 200, 400, and 600 nm, corresponding to antidot densities (AD) of about 24%, 12%, and 9%, respectively. The AD was obtained as the ratio between the areas of the patterned region and the total area of the sample. The antidot squareness and depth profile were *in situ* characterized during the etching process by scanning ion/scanning electron microscopy.

The initial magnetic state of all the samples was established by saturating the Ni layer at 296 K with an *ex situ* magnetic field ( $H_a = 1.5$  kOe) aligned along the AF easy axis of FeF<sub>2</sub>. Subsequently, the bilayers were zero-field cooled (ZFC) through the Neel temperature of FeF<sub>2</sub> ( $T_N = 78$  K) [37] down to 30 K. Such ZFC data allows studying the inherent microscopic distribution of the unidirectional FM/AF coupling. The sign of the EB is determined by the uncompensated spins direction on the surface of each AF domain to which the interfacial FM region above is coupled during the cooling across  $T_N$ .

Direct imaging of the spin structure in both sides of the FM/AF interface in the nanostructures was performed using PEEM exploiting the XMCD effect [38] as magnetic contrast mechanism. The PEEM measurements were carried out at the 11.0.1.1 beamline of the Advanced Light Source [39]. XMCD provides layer-resolved magnetic information of the FM Ni domain structure and the *uncompensated* Fe moments (spins in one direction not matched by an opposite spin) at the Ni/FeF<sub>2</sub> interface. This is accomplished by the pixel-wise asymmetry ratio of two PEEM images sequentially recorded with left- and right-handed circular polarization at the resonant L<sub>3</sub> absorption edges of Ni (852.7 eV) and Fe (708 eV). The projection of the x-ray propagation vector onto the sample surface was aligned parallel to the [001] FeF<sub>2</sub> easy axis.

The XMCD images reflect the projection of the local magnetization on

the photon propagation vector and, thus, the bright and dark gray levels in the images correspond to opposite magnetic orientations.

## III. DOMAIN CONFIGURATIONS OF THE CONTINUOUS BILAYERS

An example of the typical ZFC domain configurations at zero field and 30 K is shown in Fig. 1. A coexistence of EB domains with opposite orientations along the [001] FeF<sub>2</sub> easy axis is observed. On the Ni images (3, 5, and 7 nm), the initial remnant saturated state (dark contrast) splits into a branched pattern of small, inverted domains with opposite orientation (bright contrast). In the Fe image (labeled “bare FeF<sub>2</sub>”) the XMCD contrast arises from opposite domains of uncompensated Fe in the AF. Note that the Fe XMCD signal disappears above  $T_N$  [Figs. 2(b) and 2(d)], ruling out the presence of an Fe-rich impurity phase and demonstrating that it truly arises from uncompensated Fe moments in the AF. These uncompensated Fe moments are, laterally, randomly distributed over the whole sample, and may extend to a depth of 20–35 Å from the FeF<sub>2</sub> surface [22,24]. The collinearity between such opposite domains was found in epitaxial FeF<sub>2</sub> [27,40] and the absolute magnetization direction is known from the strong anisotropy [29] and Ising-like character of the AF [28,29].

It should also be noted that in contrast to other AF thin films [41], the AF domain structure of FeF<sub>2</sub> (110) cannot be imaged exploiting the x-ray magnetic linear dichroism (XMLD) effect [42] at the Fe L<sub>3,2</sub> edges. This is because any AF domain lies along the single spin axis of FeF<sub>2</sub> (110), due to its Ising-like behavior [28,29] and strong anisotropy [29], and different AF domains within the same axis cannot be distinguished by XMLD (see the Supplemental Material for further details). This in turn implies that a direct correlation between the actual AF domains and those of the uncompensated Fe spins cannot be established. Nevertheless, some uncompensated Fe spins are strongly locked to the AF lattice and appear as *pinned*, thus giving rise to the large EB found in these samples (see

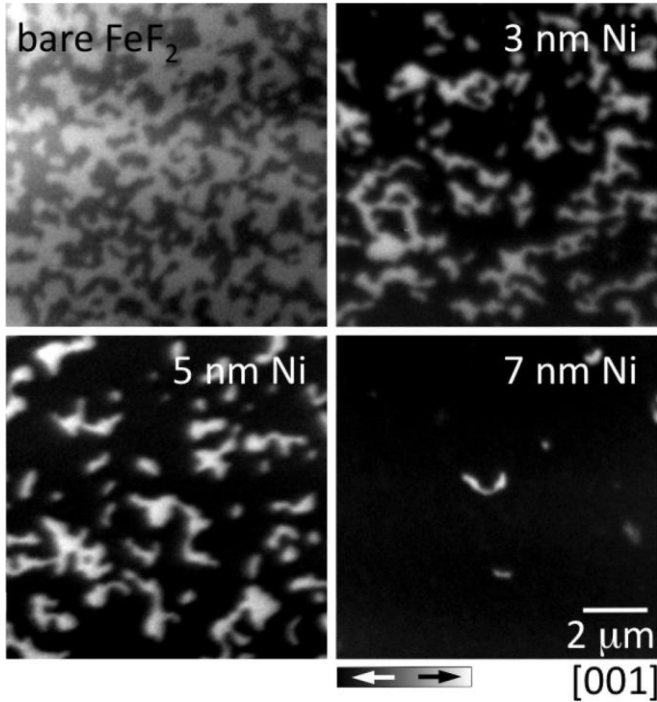
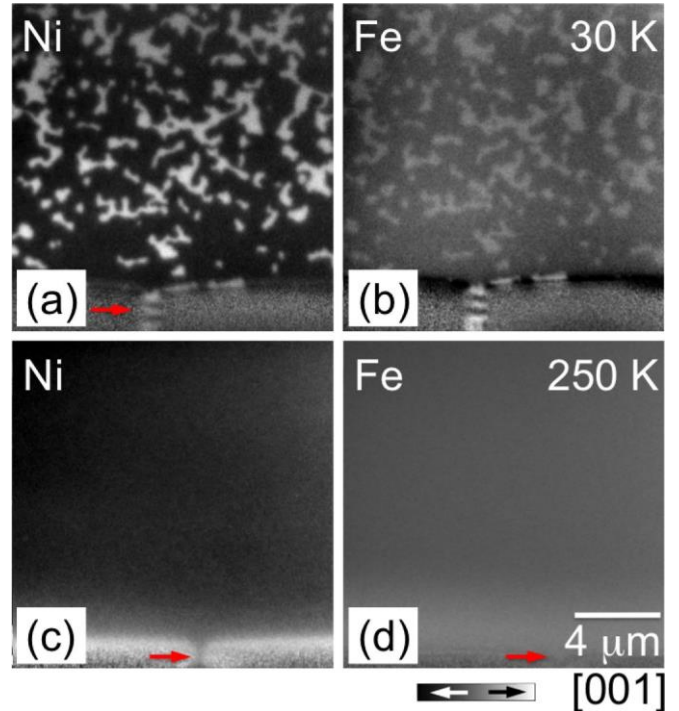


FIG. 1. XMCD images of the domain structure of the bare 70-nm-thick  $\text{FeF}_2$  layer measured at the Fe edge (top left), and of Ni (3, 5, and 7 nm)/ $\text{FeF}_2$  (70 nm) bilayers measured at the Ni edge, at zero magnetic field and 30 K upon ZFC from 296 K. The Fe image shows the typical domain structure of the uncompensated Fe moments at the surface of  $\text{FeF}_2$ . On the Ni images, the initial remnant saturated state (dark contrast) splits into a branched pattern of small, inverted domains with opposite magnetic orientation (bright contrast), as indicated by the arrows. The scale bar is the same for all images.

Figs. S3 and S4, Supplemental Material), as further discussed below.

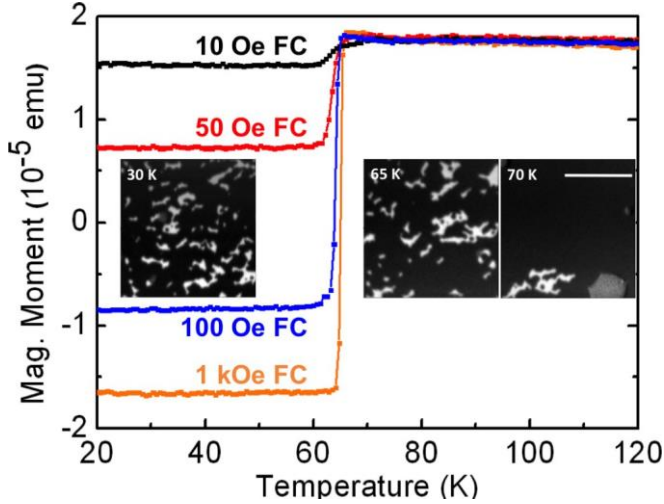
For the Ni/ $\text{FeF}_2$  bilayers, the inverted Ni domain pattern closely replicates that of the uncompensated Fe moments, regardless of the Ni thickness [Figs. 2(a) and 2(b)]. The inverted Ni domains reflect the freezing of *pinned* Fe spins in a parallel alignment to the initial Ni saturated state, in agreement with earlier XMCD observations [43]. Such pinned Fe spins induce local reversal of the overlying Ni spins when cooling through  $T_N$ . Moreover, the existence of the inverted Ni domains is by itself a direct proof of the coexistence of NEB and PEB domains after ZFC through  $T_N$  [7,9]. This finding goes beyond any previous observations where the coexistence of NEB and PEB domains could only be obtained on samples with thicker FM layers (typically 30–60 nm thick) after moderate or high field cool protocols [10,22,23,25]. Here, we thus demonstrate that the domain configuration of uncompensated spins in the AF is not unique but strongly dependent on the thickness of the FM layer. This implies that the FM actively controls the domain structure of uncompensated spins in the AF, in contrast to most theoretical models where it is assumed that once the FM layer is saturated above  $T_N$  it has no significant influence on the AF domain configuration [16–21].



The coexistence of PEB and NEB domains at the interface is reflected at the macroscopic level by the hysteresis loops at different cooling fields above and below  $T_N$ , which show

FIG. 2. (Color online) Temperature-dependent XMCD images from the same areas at the Ni and Fe edges of a Ni(4 nm)/ $\text{FeF}_2$ (70 nm) sample, measured at zero magnetic field above and below  $T_N$ . The measurements at 30 K, recorded upon ZFC from a remnant saturated state at 296 K, show how the domain structure of the uncompensated Fe moments (b) clearly replicates the inverted Ni domain pattern (a). On warming up above  $T_N$ , both the inverted Ni domains (c) and those of the uncompensated Fe spins in the AF (d) are erased. The red arrows in the images point at a defect that enables one to identify the same area in the sample. The scale bar is the same for all images.

that even for very thin Ni layers the fraction of PEB increases monotonically with the cooling field strength (Fig. S5, Supplemental Material), in agreement with observations in Ni/ $\text{FeF}_2$  bilayers with larger Ni thicknesses [44]. Furthermore, the temperature dependence of the Ni magnetization under a field-cooling process shows a clear drop around the  $T_N$  of  $\text{FeF}_2$  associated with the onset of the coexistence of PEB and NEB regions at the FM/AF interface (Fig. 3 and Fig. S6, Supplemental Material). Such drop depends on the cooling field, and the complete reversal of the Ni magnetization is reached at a large enough value where only PEB is present. The observation of full PEB unambiguously demonstrates the antiparallel coupling between the Ni moments and the *pinned*, uncompensated Fe moments in  $\text{FeF}_2$ , giving rise to the appearance of inverted domains in the FM, in agreement with micromagnetic simulations [44]. This is further confirmed by the fact that the inverted Ni domains start to appear right when the AF order in  $\text{FeF}_2$  begins to get established (insets, Fig. 3).



#### IV. STATISTICAL ANALYSIS OF THE MAGNETIC DOMAINS

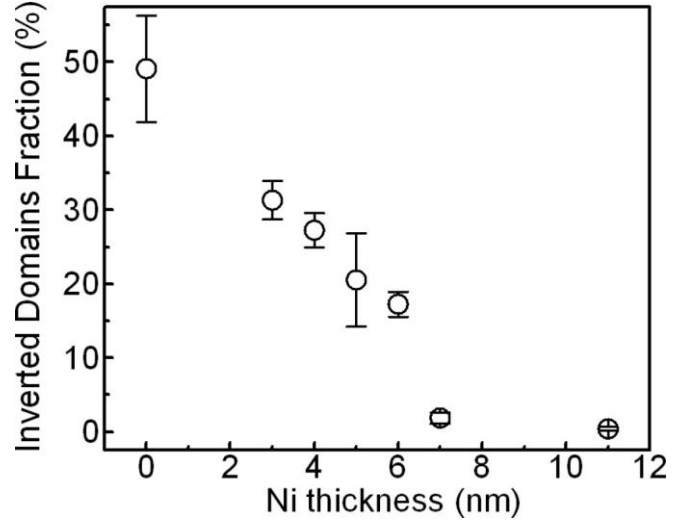
The fraction of inverted Ni domains, calculated from the ratio between the area of the imprinted bright domains below  $T_N$  and that of the initial dark domain, as well as the branched

FIG. 3. (Color online) Temperature dependence of the magnetization for different cooling fields of the Ni(6nm)/FeF<sub>2</sub>(70 nm) bilayers, showing a clear drop of the Ni magnetization below the  $T_N$  of FeF<sub>2</sub>. The drop scales with the strength of the cooling field, and the complete reversal of the Ni magnetization is reached for 1 kOe FC where only PEB is present (see also Fig. S6, Supplemental Material). The insets show XMCD images of the Ni domain structure close to the AF transition point (70 K), a few degrees below (65 K), and well below (30 K), measured at zero magnetic field upon ZFC from 296 K. The scale bar (5 $\mu$ m) is the same for the three images.

character of the domain pattern are reproducible for several series of images on different areas of the samples. The inverted Ni domains are randomly distributed throughout the whole sample (mm<sup>2</sup> sized) in each measurement, regardless of thickness. This, together with the fact that the uncompensated Fe spins replicate the inverted Ni domain pattern when cooling through  $T_N$  [Figs. 2(a) and 2(b)], indicates that the Ni/FeF<sub>2</sub> coupling is sufficiently strong to overcome the pinning by structural defects. This allows us to reach conclusions that extend beyond the specific microstructure of the samples.

To obtain quantitative, statistically meaningful results of the inverted domain fraction as a function of Ni thickness (Fig. 4), several series of Ni and Fe images were collected from three to five different areas per sample and up to three ZFC cycles per area, leading to a total of 10 to 15 independent PEEM experiments.

Close to 50% of domains with opposite orientations are found for the bare FeF<sub>2</sub> layer, as determined from the fraction of domains of uncompensated Fe spins. This is expected from an equiprobable distribution of single-domain AF crystals with their uncompensated Fe spins randomly pinned in opposite orientations throughout the mm<sup>2</sup>-sized samples. Such an uncompensated Fe spin configuration arises from the FeF<sub>2</sub>



epitaxial growth and the strong, uniaxial anisotropy [29,40]. However, a remarkable, monotonic decrease in the fraction of inverted domains with increasing Ni thickness is observed up to 7 nm. No inverted domains are imprinted for Ni thicknesses between 7 and 11 nm. This shows that reducing the FM layer thickness has a large influence on the resulting domain configuration of uncompensated spins in the AF, as further discussed below.

FIG. 4. Fraction of inverted domains for Ni/FeF<sub>2</sub>(70nm) bilayers as a function of Ni thickness, measured at zero field and 30 K, after ZFC from 296 K. The error bars represent the standard deviation of the mean but do not include smaller systematic errors arising from either the PEEM measurements (e.g., due to an inhomogeneous illumination of the XMCD images) or the analysis procedure (caused by image drift correction and evaluation of the area of the domains).

The energetic preference of a saturated FM to form very large domains of tens to hundreds of microns [45] competes with the tendency of FeF<sub>2</sub> to form small uncompensated AF domains (sub-300 nm, as shown below) close to a few crystal domains (about 30 nm) [25,33]. Therefore, the actual magnetic domain configuration is given by the balance between two contributions. First, the energy cost associated with the lateral walls of the inverted FM domains imprinted by the AF, which is proportional to the domain perimeter and scales with the FM thickness. Second, the energy decrease arising from the formation of small uncompensated AF domains in the FeF<sub>2</sub> to reduce both the magnetostatic energy and the frustration at the boundaries between the crystal domains [46]. Such energetic competition produces the branching of Ni domain walls [Figs. 1 and 2(a)] and explains why the inverted domain configuration strongly resembles the lateral structure of the underlying FeF<sub>2</sub> crystal domains. The energy cost to imprint lateral FM domain walls progressively rises as the Ni thickness increases up to 7 nm, which results in a gradual reduction of inverted domains (Fig. 4). At an upper thickness threshold between 7 and 11 nm, imprinting domains into the Ni layer is no longer energetically favorable. This is because the total energy cost for the formation of lateral domain walls through the whole FM layer thickness cannot be compensated by the energy reduction in forming small AF

domains. Our data in Fig. 4 also suggests that the rate of inverted domain formation is higher between the upper thickness threshold and 5 nm Ni than when reducing the Ni thickness below 5 nm. This is due to the fact that as the FM layer gets thinner the inversion mechanism occurs predominantly by coalescence of new inverted regions with neighboring domains rather than by nucleation of isolated domains. We note that the mean width of the isolated inverted domains (about 225 nm) is consistent with the results of earlier micromagnetic simulations which showed that the minimum critical size for the formation of such inverted domains is twice the domain wall width in the Ni layer ( $2\delta_{DW} \sim 80\text{nm}$ ) [44]. Both the mean domain width and the mean domain area (about  $350 \times 10^3 \text{ nm}^2$ ) remain constant with Ni thickness. This is associated with the existence of a characteristic size of the EB domains that best accommodates that of the AF crystal domains.

In order to get a deeper insight into this, we have analyzed the lateral *correlation length* of the inverted domains (see further below and Supplemental Material for details). For all Ni thicknesses the correlation length of the inverted domains lie with no obvious trend within the range of 190–260 nm (not shown), of the order of a few  $\text{FeF}_2$  crystal domains [25,33]. Such small crystal domains may produce a large number of pinned uncompensated spins at the boundaries which gives origin to the large EB found in these samples [6,7,34] (Figs. S3 and S4, Supplemental Material). Note that our observations do not rule out the existence of individual domains with sizes below the PEEM lateral resolution of about 40 nm.

The *unpinned* (field rotatable) and *pinned* Fe spins cannot be distinguished using zero applied field PEEM measurements and XMCD provides only an average of the two spin types. However, since the unpinned Fe spins have an effective anisotropy comparable to that of Ni which is about 100 times smaller than that of  $\text{FeF}_2$  [29], they remain oriented along the FM while cooling through  $T_N$ . Moreover, as is well known, unpinned moments do not contribute to the formation of EB domains [43,47]. Therefore, the observation of EB domains by itself is an indirect signature of *pinned* uncompensated Fe spins.

## V. EFFECT OF THE ANTIDOT PATTERNING

To further investigate the effect of spatial confinement on the coexistence of opposite EB domains, we disrupted the magnetic order by patterning the  $\text{Al}(2\text{nm})/\text{Ni}(6\text{nm})/\text{FeF}_2(70\text{nm})$  heterostructures into square arrays of square antidots (see Experimental Methods) [14,36]. The initial magnetic state of the samples was again established by first saturating the Ni layer at room temperature with an *ex situ* magnetic field ( $H_a = 1.5\text{kOe}$ ). In addition to ZFC (see Experimental Methods), FC in a small cooling field ( $H_{FC} = 50 \text{ Oe}$ ) was performed in the 200 K to 45 K range followed by ZFC to 30 K (for example, see Fig. S9, Supplemental Material). Under ZFC, a remarkable increase in the fraction of inverted Ni domains is found for patterns with AD of 24%, while in patterns with AD

12% the fraction of inverted domains is constant and comparable to that of the continuous films (Fig. 5). Thus, for AD 12% the distance between antidots is too large to destabilize the FM state thereby not favoring the formation of additional inverted domains. In contrast, for AD = 24% the size of the initial, saturation remnant state is limited by the geometrical constrictions imposed by the periodic antidot lattice. Thus, the formation of additional inverted Ni domains better matching the  $\text{FeF}_2$  magnetic microstructure is energetically favored. Therefore, the antidot separation imposes a maximum threshold for the lateral correlation length of the inverted domains, as further discussed below. Moreover, a careful observation of the PEEM images in Fig. 5 seems to

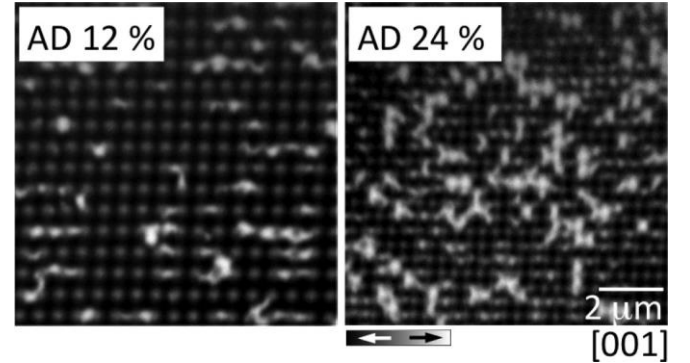


FIG. 5. XMCD images at the Ni edge of the domain structure of square arrays of 200 nm in length square antidots with antidot densities AD = 12 and 24% patterned into a  $\text{Ni}(6\text{nm})/\text{FeF}_2(70\text{nm})$  sample, measured at zero field and 30 K after ZFC from 296 K. The arrows indicate the magnetization direction. Note that the gray contrast represents the absence of XMCD signal at the position of the antidots. The scale bar is the same for both images.

indicate a preferential formation of lateral domains near the antidot edges rather than in the space in between.

A quantitative, *statistical* analysis shows that upon FC, the fraction of inverted domains is always enhanced as compared to the ZFC case. This enhancement is more pronounced in the patterned samples than in the unpatterned regions (Fig. 6).

During FC, the Zeeman energy of pinned uncompensated spins locally overcomes the exchange energy at the FM/AF interface. This promotes the formation of additional EB domains along the applied field direction (i.e., PEB domains) that imprint inverted domains in the FM. This implies the

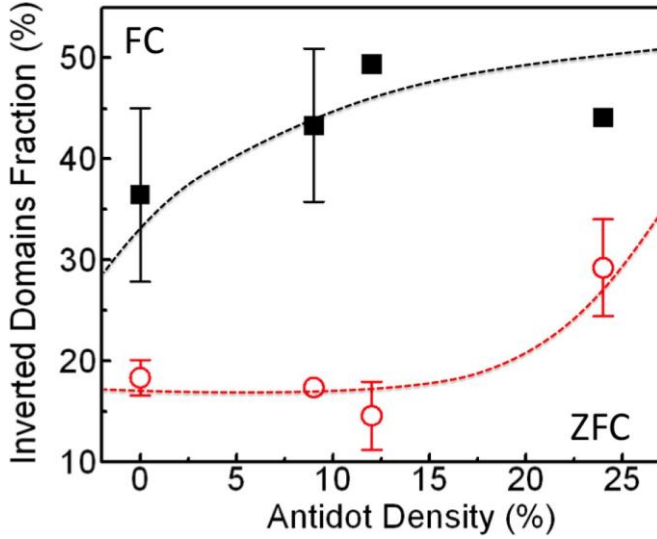


FIG. 6. (Color online) Fraction of inverted domains for Ni(6nm)/FeF<sub>2</sub>(70nm) as a function of the AD, measured at zero field and 30 K, upon ZFC from 296 K (red) and FC (black; H<sub>FC</sub> = 50 Oe from 200 K to 45 K and H<sub>FC</sub> = 0 Oe from 45 K to

30 K). The error bars represent the standard deviation over up to 15 independent measurements. The occasional data points where no error bar is given refer as to cases where a comparable statistics is not available. The dashed lines are guides to the eye.

presence of additional *pinned* uncompensated spins on the artificially created exposed lateral AF walls as a result of the antidot carving [14]. Since these additional spins are not in direct contact with the FM, they contribute to the Zeeman energy but not to the interfacial exchange energy. These spins favor the formation of inverted domains at lower values of the cooling field, in agreement with the interpretation of earlier magnetoresistance measurements [14].

## VI. LATERAL CORRELATION LENGTH

The lateral correlation length of the inverted domains imprinted by the AF into the FM layer was determined for each image using a radial distribution function analysis. An ImageJ macro [48] is employed to calculate the radial average of the pair correlation of all pairs of bright pixels as a function of distance. Such a pair correlation function is related to the probability of finding a bright pixel at a given distance from another bright pixel. The resulting pair correlation curves (see Fig. S10, Supplemental Material) are found to fit well to a single exponential decay from which the correlation lengths (D in Fig. S10, Supplemental Material) are directly obtained.

A progressive reduction of the lateral correlation length with increasing AD is observed (Fig. 7). The correlation lengths are comparable for both FC and ZFC protocols. This indicates that the size of the nucleation sites of the inverted domains is constant regardless of the thermomagnetic history of the samples. Contrary to the above-mentioned lack of trend with FM thickness on the nonpatterned samples, the fact that the correlation length of the FM domains decreases with

increasing AD implies that laterally constraining the FM/AF heterostructure by patterning may be an effective way to fine-tune the critical size for EB [3]. This could be of relevance in spintronic devices and ultrahigh-density information storage media.

## VII. CONCLUDING REMARKS

We show that confining the physical dimensions and geometry of exchange-biased Ni/FeF<sub>2</sub> bilayers, either through FM thickness variation or via patterning the whole FM/AF heterostructure, can be used to actively control the domain configuration of uncompensated spins in the AF. Imaging the spin configurations in both sides of the FM/AF interface uniquely probes the role of domain size and the competing interfacial exchange coupling and lateral contributions in a *model* EB system. For thin FM layers (below about 10 nm) competing interactions with the proximal AF system lead to tunable configurations of coexisting EB domains with opposite orientations, even in the absence of a cooling field. Antidot patterning of the Ni/FeF<sub>2</sub> heterostructures destabilizes the FM

state by geometrically constraining the heterostructure in two

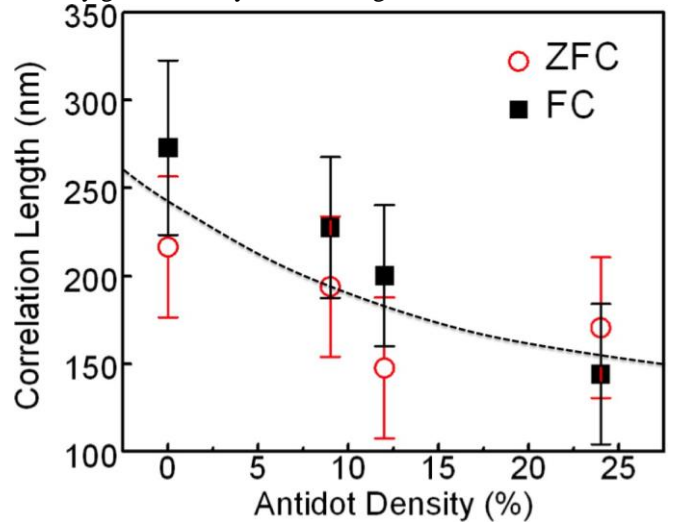


FIG. 7. (Color online) Correlation length of the inverted domains for Ni(6nm)/FeF<sub>2</sub>(70nm) as a function of the AD, measured at zero field and 30 K, upon ZFC from 296 K (red) and FC (black; same protocol as in Fig. 6). The dashed line is a guide to the eye.

dimensions. This favors the formation of additional inverted Ni domains below a critical antidot separation of the order of a few FeF<sub>2</sub> crystal domains. While a minor influence of piezomagnetism in the EB effect cannot be excluded [40,49], we believe the underlying mechanism of the AF domain formation in Ni/FeF<sub>2</sub> may be generic to other magnetic systems with complex noncollinear FM/AF spin structures, thus contributing to a more general understanding of the origin of exchange bias.



## ACKNOWLEDGMENTS

This work was supported by Spanish MINECO (MAT201233037 and FIS2013-45469), Catalan DURSI (2009SGR856, 2014SGR220), European Union FEDER funds (Una manera de hacer Europa), UPV/EHU UFI11/23, and the 7th European Union Framework Programme (FP7-PEOPLE-2012-IRSES, Project No. 318901). A.F.R. acknowledges support from the MICIIN ‘‘Ramon y Cajal’’ Programme and X.B. that from the

- University of Barcelona (UB). The work at UCSD was supported by the Office of Basic Energy Science, U.S. Department of Energy, BES-DMS funded by the Department of Energy’s Office of Basic Energy Science, and DMR under Grant No. DEFG0287ER-45332. The Advanced Light Source is supported by the Director, Office of Science, Office of Basic Energy Sciences, of the U.S. Department of Energy under Contract No. DE-AC02-05CH11231. S. Estrade and F. Peiro´ (UB) are gratefully acknowledged for the TEM images.
- Zhang, K. Chesnel, J. B. Kortright, S. K. Sinha, and I. K. Schuller, *Phys. Rev. Lett.* **95**, 047201 (2005).
- [23] R. Morales, Z-P. Li, O. Petravic, X. Batlle, and I. K. Schuller, *Appl. Phys. Lett.* **89**, 072504 (2006).
- [24] M. R. Fitzsimmons, B. J. Kirby, S. Roy, Z-P. Li, I. V. Roshchin, S. K. Sinha, and I. K. Schuller, *Phys. Rev. B* **75**, 214412 (2007).
- [25] M. R. Fitzsimmons, D. Lederman, M. Cheon, H. Shi, J. Olamit, I. V. Roshchin, and I. K. Schuller, *Phys. Rev. B* **77**, 224406 (2008).
- [26] J. W. Stout and S. A. Reed, *J. Am. Chem. Soc.* **76**, 5279 (1954).
- [27] R. A. Erickson, *Phys. Rev.* **90**, 779 (1953).
- [28] J. Stremper, U. Rutt, and W. Jauch, *Phys. Rev. Lett.* **86**, 3152 (2001).
- [29] M. T. Hutchings, B. D. Rainford, and H. J. Guggenheim, *J. Phys. C: Solid State Phys.* **3**, 307 (1970).
- [30] D. P. Belanger, P. Nordblad, A. R. King, V. Jaccarino, L. Lundgren, and O. Beckman, *J. Magn. Magn. Mater.* **31-34**, 1095 (1983).
- [31] H. Ohldag, H. Shi, E. Arenholz, J. Stohr, and D. Lederman, *Phys. Rev. Lett.* **96**, 027203 (2006).
- [32] A. Scholl, M. Liberati, E. Arenholz, H. Ohldag, and J. Stohr, *Phys. Rev. Lett.* **92**, 247201 (2004).
- [33] H. Shi and D. Lederman, *Phys. Rev. B* **66**, 094426 (2002).
- [34] J. Olamit, Z-P. Li, I. K. Schuller, and K. Liu, *Phys. Rev. B* **73**, 024413 (2006).
- [35] See Supplemental Material at <http://link.aps.org/supplemental/10.1103/PhysRevB.92.174417> for structural and magnetometry characterization of the Ni/FeF<sub>2</sub> bilayers; fabrication and topographic characterization of the Ni/FeF<sub>2</sub> antidot arrays; XMLD images of the FeF<sub>2</sub> layer; XMCD images under field cool of the Ni/FeF<sub>2</sub> antidot arrays; example of evaluation of the lateral correlation length.
- [36] M. Kovylyna, M. Erekhinsky, R. Morales, I. K. Schuller, A. Labarta, and X. Batlle, *Nanotechnology* **21**, 175301 (2010).
- [37] G. K. Wertheim and D. N. E. Buchanan, *Phys. Rev.* **161**, 478 (1967).
- [38] A. Scholl, H. Ohldag, F. Nolting, J. Stohr, and H. Padmore, *Rev. Sci. Instrum.* **73**, 1362 (2002).
- [39] A. Doran, M. Church, T. Miller, G. Morrison, A. T. Young, and A. Scholl, *J. Electron Spectrosc. Relat. Phenom.* **185**, 371 (2012).
- [40] J. Nogues, T. J. Moran, D. Lederman, I. K. Schuller, and K. V. Rao, *Phys. Rev. B* **59**, 6984 (1999).
- [1] J. Nogues and I. K. Schuller, *J. Magn. Magn. Mater.* **192**, 203 (1999).
- [2] M. Kiwi, *J. Magn. Magn. Mater.* **234**, 584 (2001).
- [3] J. Nogues, J. Sort, V. Langlais, V. Skumryev, S. Suri´nach, J. S.´ Munoz, and M. D. Bar´o, *Phys. Rep.* **422**, 65 (2005).
- [4] X. Sun, N. Frey Huls, A. Sigdel, and S. Sun, *Nano Lett.* **12**, 246 (2012).
- [5] J. Allibe, S. Fusil, K. Bouzehouane, C. Daumont, D. Sando, E. Jacquet, C. Deranlot, M. Bibes, and A. Barthel´emy, *Nano Lett.* **12**, 1141 (2012).
- [6] J. Nogues, D. Lederman, T. J. Moran, and I. K. Schuller, *Phys. Rev. Lett.* **76**, 4624 (1996).
- [7] I. V. Roshchin, O. Petravic, R. Morales, Z.-P. Li, X. Batlle, and I. K. Schuller, *Europhys. Lett.* **71**, 297 (2005).
- [8] O. Petravic, Z-P. Li, I. V. Roshchin, M. Viret, R. Morales, X. Batlle, and I. K. Schuller, *Appl. Phys. Lett.* **87**, 222509 (2005).
- [9] R. Morales, M. Velez, O. Petravic, I. V. Roshchin, Z-P. Li, X.´ Batlle, J. M. Alameda, and I. K. Schuller, *Appl. Phys. Lett.* **95**, 092503 (2009).
- [10] M. Kovylyna, M. Erekhinsky, R. Morales, I. K. Schuller, A. Labarta, and X. Batlle, *Appl. Phys. Lett.* **98**, 152507 (2011).
- [11] I. V. Roshchin, O. Petravic, R. Morales, Z.-P. Li, X. Batlle, and I. K. Schuller, International Patent Number: 05803831.6 1214 PCT/US2005025129 (2005).
- [12] R. Morales, M. Kovylyna, I. K. Schuller, A. Labarta, and X. Batlle, *Appl. Phys. Lett.* **104**, 032401 (2014).
- [13] Y. Henry, S. Mangin, T. Hauet, and F. Montaigne, *Phys. Rev. B* **73**, 134420 (2006).
- [14] M. Kovylyna, M. Erekhinsky, R. Morales, J. E. Villegas, I. K. Schuller, A. Labarta, and X. Batlle, *Appl. Phys. Lett.* **95**, 152507 (2009).
- [15] Z-P. Li, R. Morales, and I. K. Schuller, *Appl. Phys. Lett.* **94**, 142503 (2009).
- [16] A. P. Malozemoff, *Phys. Rev. B* **35**, 3679(R) (1987).
- [17] D. Mauri, H. C. Siegman, P. S. Bagus, and E. Kay, *J. Appl. Phys.* **62**, 3047 (1987).
- [18] M. Kiwi, J. Mej´ıa-Lopez, R. D. Portugal, and R. Ra´mirez, *Appl. Phys. Lett.* **75**, 3995 (1999).
- [19] K. Takano, R. H. Kodama, A. E. Berkowitz, W. Cao, and G. Thomas, *Phys. Rev. Lett.* **79**, 1130 (1997).
- [20] T. C. Schulthess and W. H. Butler, *Phys. Rev. Lett.* **81**, 4516 (1998).
- [21] K. O’Grady, L. E. Fernandez-Outon, and G. Vallejo-Fernandez, *J. Magn. Magn. Mater.* **322**, 883 (2010).
- [22] S. Roy, M. R. Fitzsimmons, S. Park, M. Dorn, O. Petravic, I. V. Roshchin, Z.-P. Li, X. Batlle, R. Morales, A. Misra, X.

- [41] S. Czekaj, F. Nolting, L. J. Heyderman, P. R. Willmott, and G. van der Laan, *Phys. Rev. B* **73**, 020401(R) (2006).
- [42] J. Stohr, A. Scholl, T. J. Regan, S. Anders, J. Lüning, M. R. Scheinfein, H. A. Padmore, and R. L. White, *Phys. Rev. Lett.* **83**, 1862 (1999).
- [43] E. Arenholz, K. Liu, Z.-P. Li, and I. K. Schuller, *Appl. Phys. Lett.* **88**, 072503 (2006).
- [44] M. Kovylnina, R. Morales, A. Labarta, and X. Batlle, *Phys. Rev. B* **86**, 224414 (2012).
- [45] A. Hubert and R. Schafer, *Magnetic Domains—The Analysis of Magnetic Microstructures* (Springer, Berlin, 1998), Chap. 3.
- [46] A. S. Morosov and A. S. Sigov, *Phys. Solid State* **46**, 395 (2004). [47] H. Ohldag, A. Scholl, F. Nolting, E. Arenholz, S. Maat, A. T. Young, M. Carey, and J. Stohr, *Phys. Rev. Lett.* **91**, 017203 (2003).
- [48] Paul Baggethun and Michael Schmid, ImageJ macro that calculates the radial average of the autocorrelation of a (binary) image,  
[http://imagejdocu.tudor.lu/doku.php?id=macro:radially\\_averaged\\_autocorrelation](http://imagejdocu.tudor.lu/doku.php?id=macro:radially_averaged_autocorrelation).
- [49] C. Binek, X. Chen, A. Hochstrat, and W. Kleeman, *J. Magn. Mater.* **240**, 257 (2002).